Impact Factor (SJIF): 6.092 E-ISSN: 2583-1615

International Journal of Research in Academic World

Received: 22/November/2023 IJRAW: 2023; 2(12):109-116 Accepted: 31/December/2023

A Study of Zinc Oxide Nanoparticles: Evaluation of Structural, Magnetic, Antibacterial and Anticancer Activities

[*1]SS Nawab Ali, [2]A Faritha, [3]A Sheik Dawood and [4]M Mohamed Sihabudeen

[*1, 2, 3]PG and Research Department of Chemistry, Thanthai Periyar Government Arts and Science College (Autonomous), Affiliated to Bharathidasan University, Tiruchirappalli, Tamil Nadu, India.

[4]PG and Research Department of Chemistry, Jamal Mohamed College (Autonomous), Affiliated to Bharathidasan University, Tiruchirappalli, Tamil Nadu, India.

Abstract

Zinc oxide nanoparticles were synthesized by green chemistry method. Formations of nanoparticles were characterized by various spectroscopic analysis. Synthesized that nanoparticles exhibits nano flower like structure using X-ray diffraction pattern. Morphology and chemical composition were identified through field emission scanning electron microscopy and energy dispersive x-ray analysis spectra. In the case of Fourier transform infra-red spectra, the Zinc oxide vibration observed at 618 cm-1 for ZnO NPs. Optical study was determined by and PL spectra. Diamagnetic behavior was observed synthesized ZnO NPs using VSM analysis. The native defect was identified by EPR studies. The antibacterial properties of the ZnO NPs were examined by Gram positive and Gram negative strains.

Keywords: ZnO nanoparticles, XRD, VSM, EPR, antibacterial activity

Introduction

The Zinc oxide nanoparticles are important II-VI semiconductor for direct band gap 3.36 eV at room temperature and n-type semiconductor with large exciton binding energy of 60 meV. ZnO NPs are potential application in optoelectronics, photonics [Singh *et al*., 2009; Alaria, *et al*., 2005; Sharma *et al*., 2003 and Sluiter *et al*., 2005], cosmetic pigments, surface acoustic wave devices, varistors, optical materials, catalyst, ultraviolet absorbers [Chavillon *et al*., 2011] and biomedical applications [Tam *et al*., (2011); Bintsis *et al*., (2000) and Brayner *et al*., (2006)].

Metal oxide nanoparticles are the most widely used antibacterial and antifungal agent in the food industry applications [Raja *et al*., (2018)]. ZnO NPs displays biocidal activity against a broad range of Gram positive and Gram-negative microorganisms [Haja Hameed *et al*., (2013)]. The antimicrobial activity of ZnO NPs is mainly based on the following mechanisms: (a) release of Zn^{2+} ions which bind to electron donor groups in molecules containing sulphur, oxygen or nitrogen, (b) disruption of DNA replication and, (c) oxidative stress through the catalysis of reactive oxygen species (ROS) formation [Haja Hameed *et al*., (2016)]. ROS contain the most reactive hydroxyl radical (OH), the less toxic superoxide anion radical ($^{\cdot}O_2^-$) and hydrogen peroxide with a weaker oxidizer (H_2O_2). This can damage DNA, cell membranes, etc., leading to cell death [Foster *et al*., 2012].

The ROS, such as superoxide anions and hydrogen peroxide (H_2O_2) are normal by products of cellular aerobic metabolism. The superoxide anions ($^{\cdot}O_2^-$) are secondarily converted to (H_2O_2) by the superoxide dismutase (SOD). H_2O_2 has a dual role in cellular homeostasis. The low level of intracellular H_2O_2 stimulated cell growth [Sundaresan *et al*; 1995], whereas high levels of H_2O_2 led to cellular senescence and apoptosis [Bernard *et al*; 2004]. The conduction electrons and valence holes in semiconductors such as ZnO have been traditionally used for photocatalytic oxidation of organic and inorganic pollutants, and as sensitizers for photo-destruction of cancer cells [Cai *et al*; 1991, Kubota *et al*; 1994] via oxidative damage. The electrons and holes were typically produced via UV irradiation and excitation. When NPs are synthesized by using specialized methods, more numbers of holes and/or electrons might be available even without the presence of UV light. The holes are powerful oxidants and they can react with water or surface-bound chemisorbed hydroxyl groups to produce hydroxyl radicals. The conduction band electrons are good reductants, and can move to the particle surface and be trapped in metastable surface states, or react with electron acceptors or oxidants such as adsorbed O_2. The various activated oxygen species can be produced by the reactions of holes and electrons in a metal oxide semiconductor, where ROS play crucial role in eukaryotic cell death by ZnO NPs.

***Corresponding Author:** SS Nawab Ali

Experimental Methods

- **Synthesis**

The following high purity chemicals such as Zinc nitrate, and NaOH were used as precursors without further purification.

ZnO nanoparticles was prepared by Microwave-assisted method. In this method, a solution was prepared by dissolving 0.1 M of Zinc nitrate in double distilled water. In order to use NaOH solution as a precipitating agent, 0.1M of NaOH solution was added into the solution. Then, the white precipitate was obtained. The white precipitate was stirred at room temperature for 20 minutes. The resultant solution was transferred to poly propylene capped autoclave bottles. Then, the solution was irradiated by microwave with the power of 800 W for 10 min. After forming solution was cooled into the room temperature. The solution was washed several times with double distilled water and ethanol. The precipitate was dried at 120˚C. After that the ZnO NPs was annealed at 800 ˚C for 5 hours and then analyzed for further studies. The schematic diagram for the preparation of the ZnO NP samples is shown in Fig. 1.1.

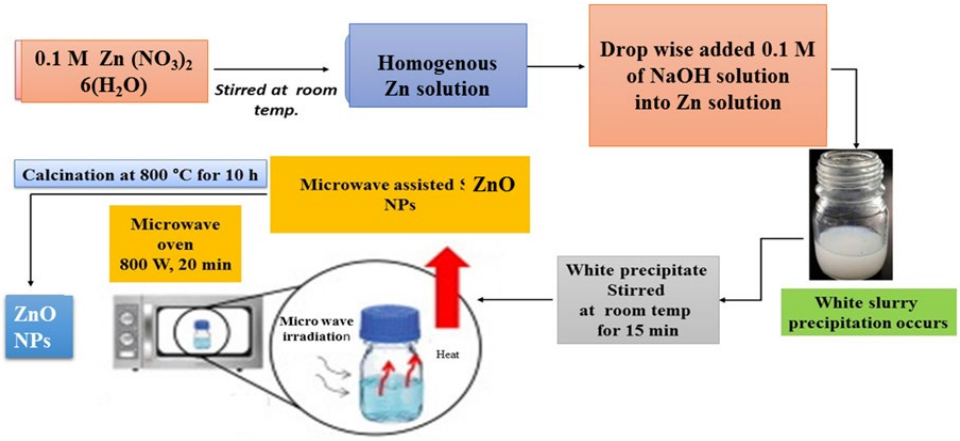

Fig 1: Schematic diagram for the formation of ZnO NPs.

Antibacterial assay

The antibacterial activity of the ZnO NPs was studied against gram positive G+ (*Staphylococcus aureus*, *Streptococcus pneumoniae and Bacillus subtilis*) and gram negative G- (*Klebsiella pneumoniae, Shigella dysenteriae, Escherichia coli, Pseudomonas aeruginosa* and *Protus vulgaris*) bacterial strains using the well diffusion method. Petri plates were prepared with 25 ml of sterile Muller Hinton agar (MHA, Himedia) and each bacterial pathogen was individually swabbed on MHA in separate plates. The antibacterial activity was tested at a concentration of 2 mg/ml with the required quantity of the ZnO NPs dispersed in dimethyl sulphoxide (DMSO). The zone of inhibition levels (mm) was measured after 24 h, it was incubated overnight at 37 °C. The standard antibiotic Amoxicillin was used as the positive control.

Anticancer assay

- **Cell Culture:** MCF-7 (Human breast carcinoma cells) cell line were cultured in liquid medium (DMEM) supplemented 10% Fetal Bovine Serum (FBS), 100 u/ml penicillin and 100 µg/ml streptomycin, and maintained under an atmosphere of 5% CO_2 at 37 ºC.
- **MTT Assay:** The ZnO NPs was tested for *in vitro* cytotoxicity, using MCF-7 cells by 3-(4,5-dimethylthiazol-2-yl)-2,5-diphenyltetrazolium bromide (MTT) assay. Briefly, the cultured MCF-7 cells were harvested by trypsinization, pooled in a 15 ml tube. Then, the cells were plated at a density of 1×10^5 cells/ml cells/well (200 µL) into 96-well tissue culture plate in DMEM medium containing 10% FBS and 1% antibiotic solution for 24-48 hour at 37 °C. The wells were washed with sterile PBS and treated with various concentrations of the ZnO NPs in a serum free DMEM medium. Each sample was replicated three times and the cells were incubated at 37°C in a humidified 5% CO_2 incubator for 24 h. After the incubation period, MTT (20 µL of 5 mg/ml) was added into each well and the cells incubated for another 2-4 h until purple precipitates were clearly visible under an inverted microscope. Finally, the medium together with MTT (220 µL) were aspirated off the wells and washed with 1X PBS (200 µl). Furthermore, to dissolve formazan crystals, DMSO (100 µL) was added and the plate was shaken for 5 min. The absorbance for each well was measured at 570 nm using a micro plate reader (Thermo Fisher Scientific, USA) and the percentage cell viability and IC_{50} value was calculated using Graph Pad Prism 6.0 software (USA).

Characterization studies

- **X-ray Powder Diffraction (XRD) Studies:** The XRD patterns of the ZnO NPs was collected using a X'PERT PRO PAN alytical X-ray diffractometer with CuKα (40 kV, 30 mA) radiation source. The ZnO NPs was gently crushed before being smeared on a clean glass slide. The powder diffraction patterns were collected over 2θ in the range between 10˚-80˚ with a scan speed and sampling width of 2 min^{-1} and 0.05˚ respectively**.**
- **Field Emission Scanning Electron Microscope (FESEM) Studies:** FESEM was performed on the ZnO sample using a Carl Zeiss Ultra 55 FESEM microscope operating at 30 kV. The microscope was equipped with a charge-coupled device (CCD) camera. The samples were prepared by using 1mg of ZnO NPs samples coated with 1.2 nm gold particle separation on a carbon tape using the low vacuum.
- **Energy Dispersive Analysis of X-ray Spectroscopy (EDAX) Studies:** Energy dispersive analysis of X-ray spectroscopy was done using an EDAX (model: Inca) with FEI-QUANDA 200F high resolution scanning electron microscope operated at 30 kV. Dry powdered samples were attached to the substrate using a double-sided carbon tape and mounted onto the sample holder.
- **Fourier Transform Infra-red (FT-IR) Spectroscopy studies:** A Perkin-Elmer Fourier transform infra-red (FT-IR) spectrometer was used in transmission mode and the

corresponding spectra were recorded in the range of 4000-400 cm^{-1} using the KBr pellet technique for ZnO sample.

- **UV-Visible Spectroscopy Studies:** The absorption spectra of ZnO NPs was studied in the range between 200 and 800 nm by Jasco 720 spectrophotometer.
- **Photoluminescence (PL) Studies:** Room temperature PL measurements were performed for ZnO NPs with excitation wavelength of 325 nm using JASCO spectrofluorometer FP-8200.
- **Vibrating Sample Magnetometer (VSM) and Electron Spin Resonance Spectrometer (EPR) Studies:** The vibrating sample magnetometer were recorded 15 kOe using as a Lakeshore VSM 7410 and Electron Spin Resonance Spectrometer were recorded using JES-FA200.

Results and Discussion

X-ray Diffraction Patterns

Figure 3.2 shows the X-ray diffractions patterns of Microwave assisted synthesis of ZnO NPs. XRD patterns of synthesized ZnO NPs exhibit hexagonal wurtzite structure. The XRD peaks at angles (2Θ) of 31.7775, 34.4498 and 36.2676 corresponding to the (100), (002) and (101) planes of the ZnO NPs, respectively. Other XRD peaks at angles (2θ), FWHM (β), hkl and Relative intensity are given in Table-3.1, which is perfectly matched with standard with JCPDS card No. 79-2205 for ZnO NPs. The lattice constant values a = 3.2516 Å and c = 5.2068 Å for ZnO NPs respectively.

The micro-strain the breadth of the Bragg peak is a combination of both instrument and sample-dependent effects. To decouple these contributions, it is necessary to collect a diffraction pattern from the line broadening of a standard material such as silicon to determine the instrumental broadening. The instrument-corrected broadening β_{hkl} [Ramakanth., (2007)] can be represented by:

$$\beta hkl = [\beta hkl^2 measured - \beta hkl^2 instrumental]^{1/2} \quad (3.1)$$

The particle grain size of ZnO NPs is determined by the X-ray line broadening method using the Scherrer's equation,

$$D = k\lambda/\beta(D\cos\theta) \quad (3.2)$$

Where D-is the size in nanometers, λ is the wavelength of the radiation (1.5406Å for CuKα), k is a constant (0.94), β_D-is the peak width at half-maximum intensity and θ is the peak position. The average crystallite size are observed at 42.47 nm for ZnO NPs.

The strain-induced broadening βε is given by the Williamson-Hall formula βε = 4εtanθ, where ε is the root mean square value of the micro-strain. Assuming that the particles size and strain contributing to the line broadening and independent of each other and both have a Cauchy like profile, the observed line width is simply the sum of these two, i.e., $\beta_{hkl} = (k\lambda/D\cos\theta) + 4\varepsilon\tan\theta$, which becomes as

$$\beta_{hkl}\cos\theta = (k\lambda/D) + 4\varepsilon\sin\theta \quad (3.3)$$

When plotting the Williamson-Hall equation between β cos θ Vs. 4sin θ, the slope of the line is the strain ε. Figures 1.3 shows the plots of Williamson-Hall equation for ZnO NPs. The calculated strain values are 0.0028.

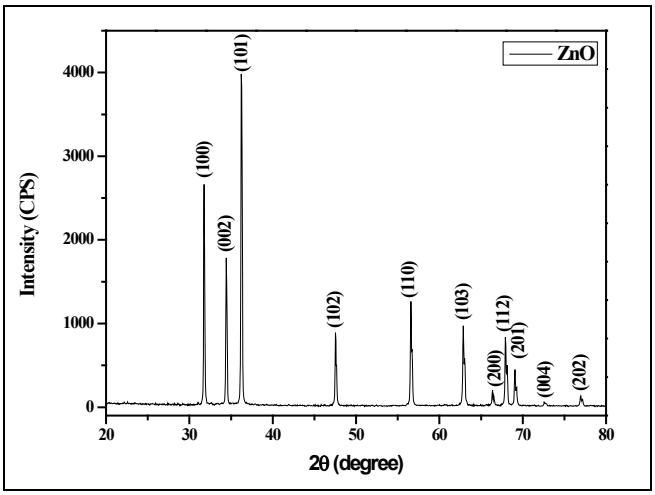

Fig 2: X-ray diffraction patterns of ZnO NPs

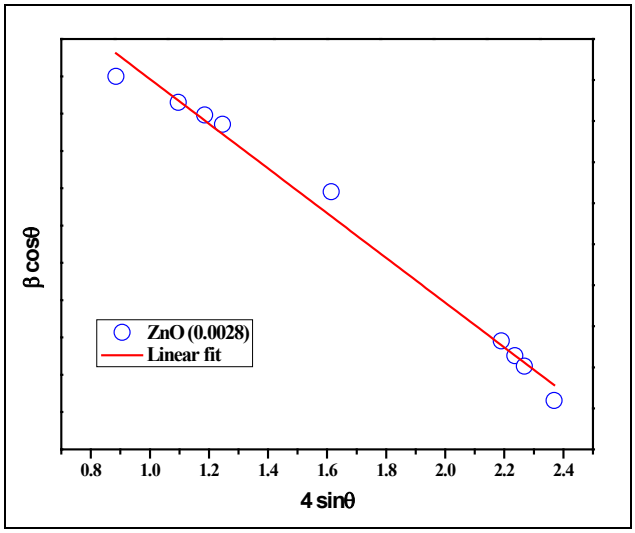

Fig 3: The Williamson-Hall plots of ZnO NPs

Table 1: X-ray diffraction parameter values of ZnO NPs as compared with JCPDS card No. 79-2205 of ZnO NPs.

JCPDS Card no: (79-2205) 2θ (degree)	ZnO 2θ (degree)	JCPDS Card no: (79-2205) d-spacing [Å]	ZnO d-spacing [Å]	ZnO FWHM β (°)	(hkl)	JCPDS Card no: (79-2205) Relative Intensity	ZnO Relative Intensity
31.79	31.7775	2.81	2.81600	0.1968	100	56.40	67.69
34.41	34.4498	2.60	2.60343	0.1476	002	41.50	41.94
36.25	36.2676	2.47	2.47701	0.1968	101	99.99	100.00
47.53	47.5670	1.91	1.91166	0.1968	102	21.10	20.96
56.59	56.5746	1.62	1.62682	0.2460	110	30.50	32.35
62.85	62.8518	1.47	1.47860	0.2460	103	26.80	23.36
66.37	66.3417	1.40	1.40904	0.1476	200	4.00	4.41
67.94	67.9225	1.37	1.37890	0.1800	112	21.70	21.21
69.08	69.0539	1.35	1.35905	0.2400	201	10.60	10.95
-	72.5934	-	1.30125	0.1800	004	3.30	1.40
	76.9305		1.23834	0.1800	202		2.95

Field Emission Scanning Electron Microscopic Studies

The surface morphology of microwave assisted synthesis of ZnO NPs was examined by FESEM analysis is shown in Fig. 1.4(a-b). FESEM images clearly show the synthesized ZnO NPs exhibits, flower like structure and average particles size in the nanoscale range. The formation of flower shape may be two reasons such as crystal nucleation and crystal growth direction. The small quantity of the growth unit ($[Zn(OH)_4]^{2-}$), which results decompose to ZnO. Subsequently, ZnO crystalline particles can be self-assembled one by one along with the [0 0 0 1] crystals direction and, by this co-ordination, the nanoflower-like ZnO morphology are formed.

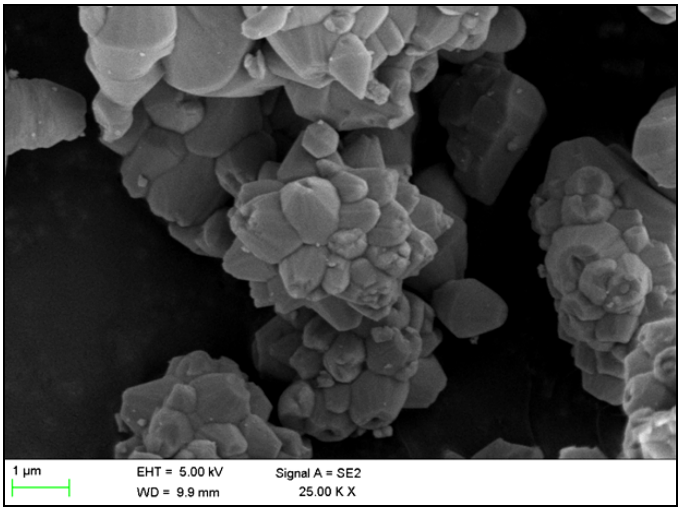

Fig 4(a): FESEM image of lower magnification of ZnO NPs

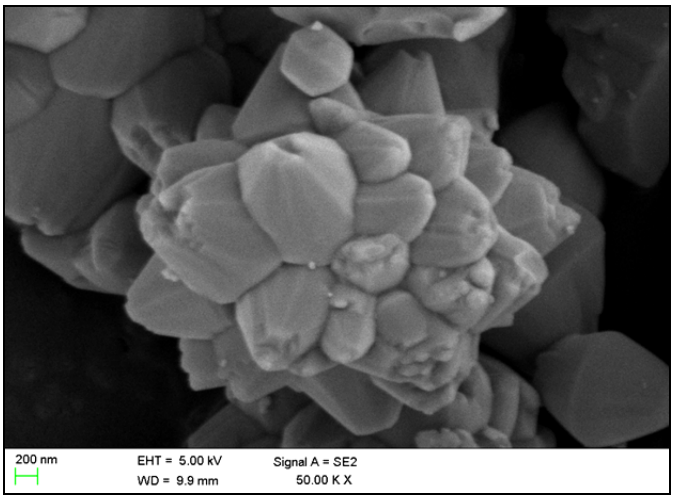

Fig 4(b): FESEM image of higher magnification of ZnO NPs

EDAX Spectroscopic Studies

The elemental composition percentage was identified by EDAX spectra is shown in Fig. 1.5. The EDAX data clearly indicates that the expected elements such as Zn, and O are present in the synthesized nanoparticles. From this analysis, the chemical compositions of Zn and O are found to be 51.49% and 48.51% respectively.

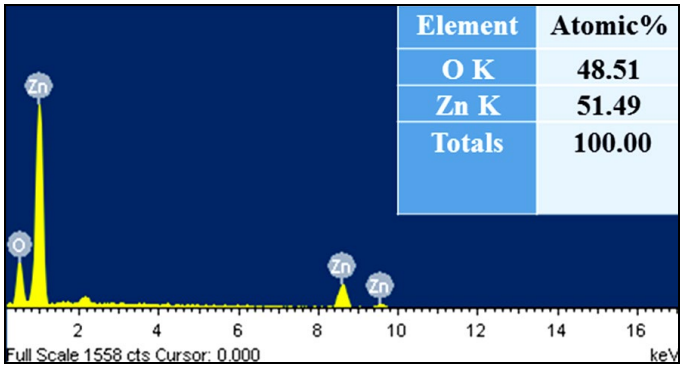

Fig 5: Elemental composition of ZnO NPs.

FTIR Spectroscopic Analysis

Figure 1.6 shows the FT-IR spectra of microwave assisted synthesized ZnO

NPs. The peak in the range of 3020-3650 cm^{-1} corresponds to the vibrational mode of O-H bonds (Zandi *et al*; 2011). The O-H stretching band observed at 3420 cm^{-1} for ZnO NPs. The peaks at 2978 and 2837 cm^{-1} are due to symmetric and asymmetric C-H [Munoz-Hernández *et al*., 2008]. The H-OH bending vibration is around at 1670 cm^{-1} for ZnO NPs. The symmetric C=O bands are observed at 1419 cm^{-1}. The asymmetric O-H stretching at 1044 and 1014 cm^{-1} for ZnO NPs. The Metal-oxygen (M-O) peaks appearing between 400 and 600 cm^{-1} [Dutta *et al*., 2008] The Zn-O stretching bands observed in 650, 621, 519 and 461 cm^{-1} [Xiong *et al*., 2006] for ZnO NPs.

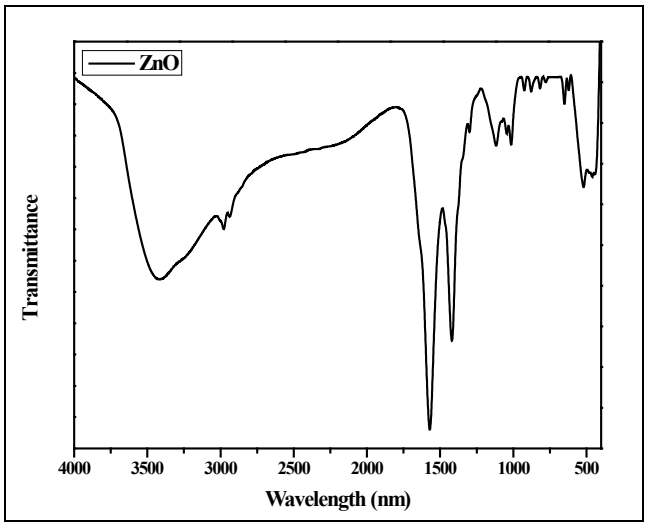

Fig 6: FT-IR spectrum of ZnO NPs

UV-Vis Reflectance Spectral Studies

The optical properties of ZnO NPs determined by UV-Visible reflectance spectroscopy, as shown in Fig. 1.7. The excitonic pecks are observed around 367 nm for ZnO NPs. The optical energy band gap of synthesized ZnO NPs is calculated by optical absorption edge onset (λ) of the reflectance spectrum by the relation E (eV) = $1240/\lambda$ nm. Whereas λ is the wavelength and E is the band gap energy of synthesized ZnO NPs. The band gap of 3.37 eV is obtained for ZnO NPs.

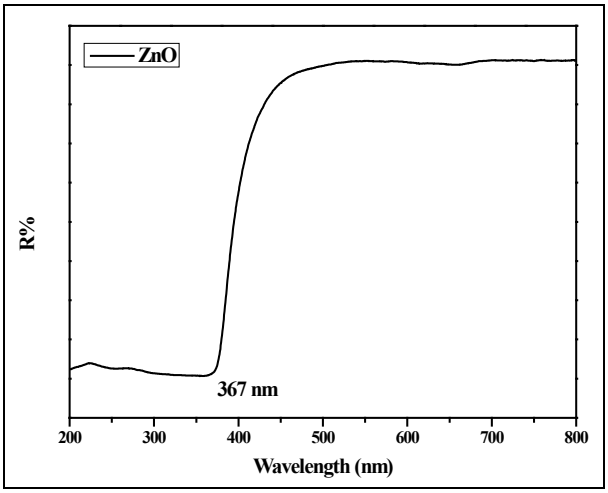

Fig 7: UV-Visible reflectance spectrum of ZnO NPs

Photoluminescence Spectral Studies

Figure 1.8 shows the PL spectrum of ZnO NPs are synthesized by Microwave-assisted method and excitation wave length of 340 nm. The UV emission corresponds to the radiative recombination of the free exciton-exciton collision process in the ZnO NPs. The violet emission observed at 415 nm, which is attributed to electron transition from a shallow donor level of the zinc interstitial to the top level of the valence band [Haja hameed *et al*., (2016)]. Three blue emission peaks observed at 425, 435 and 462 nm for ZnO NPs, due to the charge carrier transition from ZnO to the valence band or transition from the conduction band to the O_i state [Vijayaprasath *et al*., 2018]. The blue-green emission centered at 482 nm is attributed to the charge carrier transition between oxygen vacancy and interstitial oxygen [Mhlongo *et al*., (2011)].

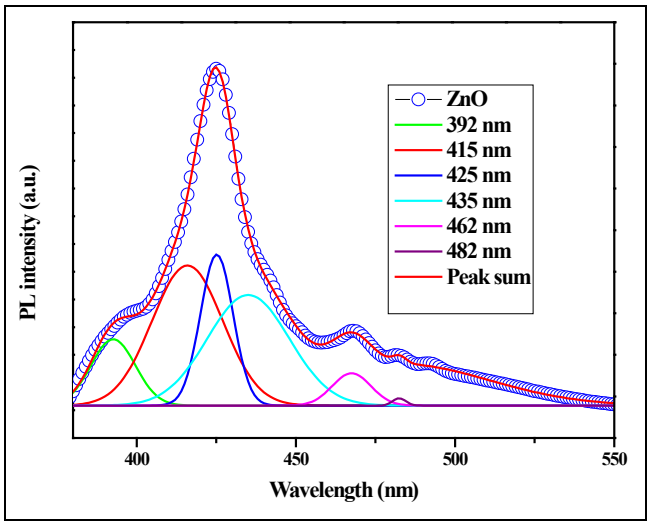

Fig 8: Photoluminescence spectrum of ZnO NPs.

VSM and EPR Spectral Studies

Magnetization Vs Magnetic field (M-H) curves of synthesized ZnO NPs samples, estimated at 300 K with an applied magnetic field range from 0 to ±15 kOe are shown in Fig.1.9. In earlier literature ZnO NPs were exhibits diamagnetic behaviours [Zhou *et al*., (2009), Vijayaprasath *et al*., (2014)]. In our results, the diamagnetic behaviours observed for pure ZnO NPs. The magnetization value observed at 15 kOe is 154.66 E^{-6} emu/g for ZnO NPs. The room temperature EPR spectra of the ZnO NPs is shown in Fig. 1.10. For the ZnO spectra are composed of an intense line at ~14370 G with the value of the g factor of about 1.925, which is due to the of Singly ionized oxygen vacancy (V_o) attributed to unpaired electrons trapped at oxygen vacancies [Kappers *et al*., (2008)].

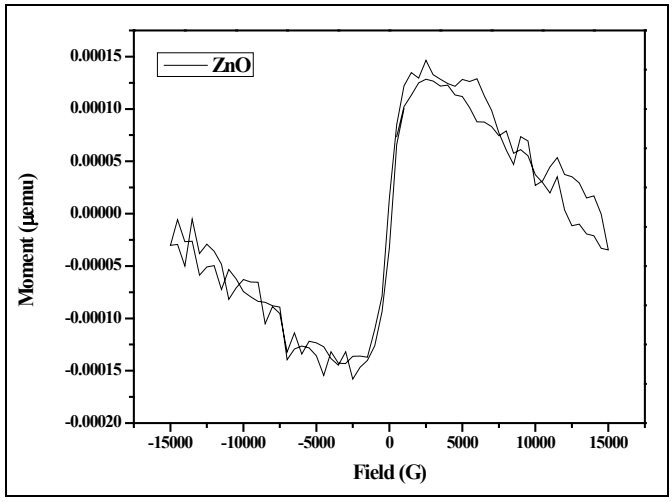

Fig 9: Magnetic Behavior of ZnO NPs

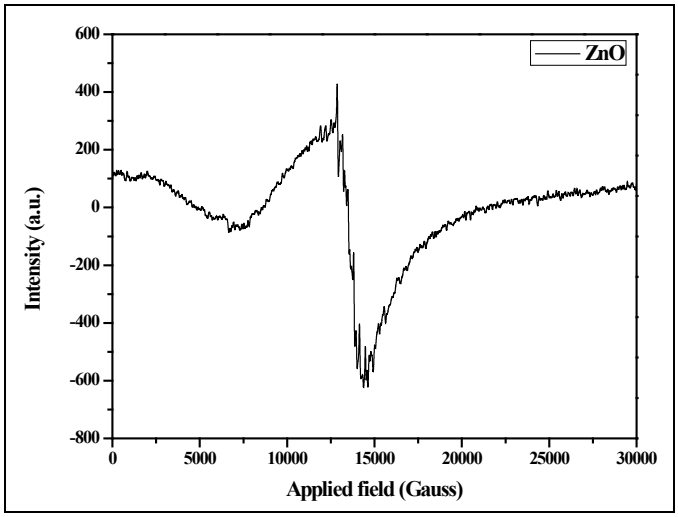

Fig 10: EPR spectrum of ZnO NPs

Antibacterial Activity

The antibacterial activity of the synthesized ZnO NPs were tested against gram positive bacteria (*S. aureus*, *S. pneumoniae and B. subtilis*) and gram negative G-(*E. coli, K. pneumoniae, P. aeruginosa, P. vulgaris and V. cholerae*) strain by agar well diffusion method. The different bacterial strains of zone inhibition as shown in Fig. 1.11. The ZnO NPs shows the antibacterial activity as compared to the standard antibiotics erythromycins pharmaceutical formulation. The Zone inhibition of bacterial cells may be due to distractions of cell membrane, is mainly due to the combination of various factors such as ROS and the release of Zn^{2+} bacteria losing the viability of cell division [Jones *et al*., (2009); Yamamoto (2001); Tam, *et al*., (2008) and Dutta *et al*., (2012)], leads to killing of bacteria.

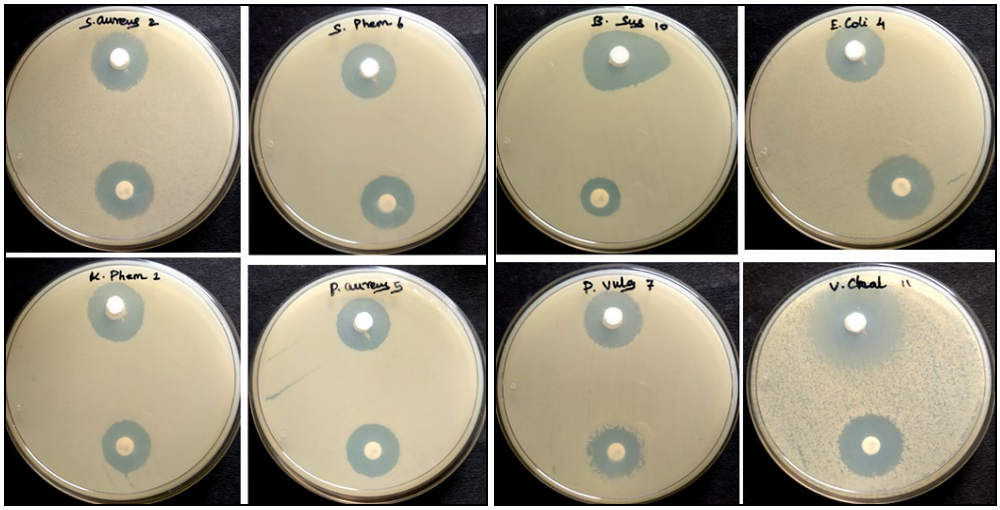

Fig 11: The Zone of inhibition for various bacterial strain treated with ZnO NPs: against gram positive bacteria (*S. aureus*, *S. pneumoniae and B. subtilis*) and gram negative bacteria (*E. coli, K. pneumoniae, P. aeruginosa, P. vulgaris and V. cholerae*).

Anticancer Studies

The MTT assay was carried out the inhibitory effects of the ZnO NPs treated against MCF-7 Breast cancer cells. MCF-7 cells were incubated with various (10-100 µg/ml) concentrations of ZnO NPs as shown in Fig. 1.12. In MTT assay, the statistical analysis revealed that ZnO NPs induced apoptosis in treating MCF-7 cells, this results indicating cell death may be apoptotic or cell death induced toxicity (ROS). The IC_{50} value of 53.68µg/ml (evaluated after 24h) of ZnO NPs against 40.79 cells was ($p \leq 0.05$ P value <0.01). Cell morphological changes were observed for light microscope with different concentration 10, 30, 50, 70 and 100 µg/ml (Fig. 1.13). The results revealed that the occurrence of morphologically altered cells observed ZnO NPs treated group as compared to control group.

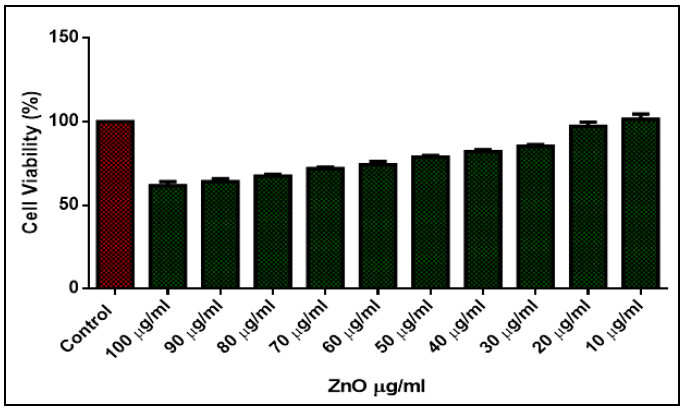

Fig 12: MTT assay of ZnO NPs treated against MCF – 7 (Breast Cancer cells)

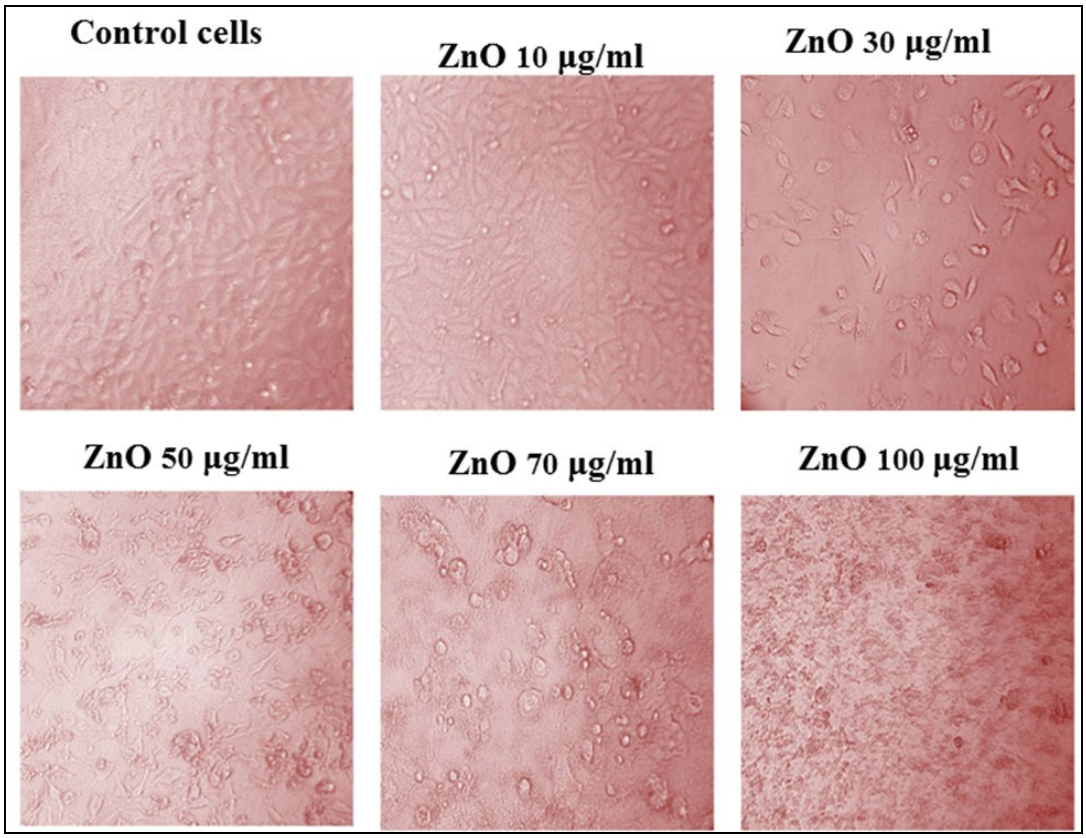

Fig 13: Cell morphological changes were observed for light microscope with different concentration 10, 30, 50, 70 and 100 µg/ml of ZnO NPs treated with human Breast cancer cell line (MCF-7).

Conclusions

In summary, the ZnO NPs were synthesized by the microwave assisted method. From the X-ray diffraction pattern revealed that synthesized NPs exhibits hexagonal wurtzite structure. FESEM image showed that synthesized ZnO NPs formed nanoflower like structure. The elemental composition were identified through EDAX spectra. From the recorded FT-IR spectra, the various vibrational frequencies was assigned for the ZnO NPs samples. The optical studies were carried out by UV-Vis and Photoluminescence spectra. The antibacterial studies performed against a G+ (*S. aureus*, *S. pneumoniae and B. subtilis*) and G-(*E. coli, K. pneumoniae, P. aeruginosa, P. vulgaris and V. cholerae*) bacterial strains showed that the ZnO NPs possessed a higher antibacterial effect than the commercial antibiotic (Amoxicillin). The ZnO NPs have been used in the treatment of pneumonia, blood stream infection, kidney failure; wound infection and urinary tract infections. The cytotoxic effect of the ZnO NPs was examined in cultured (MCF-7) human breast cancer cells, with reference to cell death, an IC_{50} concentration of 40.79 µg/ml of the ZnO NPs.

References

1. Alaria J, Turek P, Bernard M, Bouloudenine M, Berbadj A, Brihi N, Schmerber G, Colis S, Dinia A. "No ferromagnetism in Mn doped ZnO semiconductors." Chemical Physics Letters 415. 2005; 4(6):337-341.
2. Bernard D, Gosselin K, Monte D, Vercamer C, Bouali F, Pourtier A, Vandenbunder B, Abbadie C. Involvement of Rel/nuclear factor-kappB transcription factor in keratinocyte senescence, Cancer Res. 2004; 64:472-481.
3. Bintsis, Thomas, Evanthia Litopoulou-Tzanetaki, and Richard K. Robinson. "Existing and potential applications of ultraviolet light in the food industry–a critical review." *Journal of the Science of Food and Agriculture 80*. 2000; 6:637-645.
4. Brayner, Roberta, Roselyne Ferrari-Iliou, Nicolas Brivois, Shakib Djediat, Marc F. Benedetti, and Fernand Fiévet. "Toxicological impact studies based on Escherichia coli bacteria in ultrafine ZnO nanoparticles colloidal medium." Nano letters. 2006; 6(4): 866-870.
5. Cai T, Hashimoto K, Itoh K, Kubota Y, Fujishima A. Photo killing of malignant cells with ultrafine TiO_2 powder, Bull. Chem. Soc. Japan. 1991; 64:1268-1273.
6. Chavillon, Benoit, Laurent Cario, Adèle Renaud, Franck Tessier, François Cheviré, Mohammed Boujtita, Yann Pellegrin *et al*. "P-type nitrogen-doped ZnO nanoparticles stable under ambient conditions." *Journal of the American Chemical Society*. 2011; 134(1):464-470.
7. Dutta M, Mridha S, Basak D. "Effect of sol concentration on the properties of ZnO thin films prepared by sol–gel technique." Applied Surface Science. 2008; 254(9):2743-2747.
8. Dutta RK, Bhavani P. Nenavathu, Mahesh K. Gangishetty, and A. V. R. Reddy. "Studies on antibacterial activity of ZnO nanoparticles by ROS induced lipid peroxidation." Colloids and Surfaces B: Biointerfaces. 2012; (94):143-150.
9. Foster, Howard A., Iram B. Ditta, Sajnu Varghese, and Alex Steele. "Photocatalytic disinfection using titanium dioxide: spectrum and mechanism of antimicrobial activity." Applied microbiology and biotechnology. 2011; 90(6):1847-1868.
10. Gandhi, Vijayaprasath, Ravi Ganesan, Haja Hameed Abdulrahman Syedahamed, and Mahalingam Thaiyan. "Effect of cobalt doping on structural, optical, and magnetic properties of ZnO nanoparticles synthesized by coprecipitation method." The Journal of Physical Chemistry C 118. 2014; 18:9715-9725.
11. Hameed, Abdulrahman Syedahamed Haja, Chandrasekaran Karthikeyan, Seemaisamy Sasikumar, Venugopal Senthil Kumar, Subramanian Kumaresan, and Ganesan Ravi. "Impact of alkaline metal ions Mg 2+, Ca 2+, Sr 2+ and Ba 2+ on the structural, optical, thermal and antibacterial properties of ZnO nanoparticles prepared by the co-precipitation method." Journal of Materials Chemistry B. 2013; 1(43):5950-5962..
12. Hameed, Abdulrahman Syedahamed Haja, Chandrasekaran Karthikeyan, Abdulazees Parveez Ahamed, Nooruddin Thajuddin, Naiyf S. Alharbi, Sulaiman Ali Alharbi, and Ganasan Ravi. "*In vitro* antibacterial activity of ZnO and Nd doped ZnO nanoparticles against ESBL producing Escherichia coli and Klebsiella pneumoniae." Scientific reports. 2016; 6:24312.
13. Hankare PP, Chate PA, Sathe DJ, Chavan PA, Bhuse VM. "Effect of thermal annealing on properties of zinc selenide thin films deposited by chemical bath deposition." *Journal of Materials Science: Materials in Electronics*. 2009; 20(4):374-379.
14. Jones, Nicole, Binata Ray, Koodali T. Ranjit, and Adhar C. Manna. "Antibacterial activity of ZnO nanoparticle suspensions on a broad spectrum of microorganisms." FEMS microbiology letters. 2008; 279(1):71-76.
15. Kappers LA, Gilliam OR, Evans SM, Halliburton LE, Giles NC. "EPR and optical study of oxygen and zinc vacancies in electron-irradiated ZnO." Nuclear Instruments and Methods in Physics Research Section B: Beam Interactions with Materials and Atoms 266, 12-13, (2008):2953-2957.
16. Kubota Y, Shuin T, Kawasaki C, Hosaka M, Kitamura H, Cai R, Sakai H, Hashimoto K, Fujishima A. Photokilling of T-24 human bladder cancer cells with titanium dioxide,. *Br. J. Cancer*. 1994; 70:1107-1111.
17. Mhlongo GH, Ntwaeaborwa OM, Swart HC, Kroon RE, Solarz P, Ryba-Romanowski W, Hillie KT. "Luminescence dependence of Pr3+ activated SiO2 nanophosphor on Pr3+ concentration, temperature, and ZnO incorporation." The Journal of Physical Chemistry C. 2011; 115(36):17625-17632.
18. Munoz-Hernández, Gerardo, Alejandro Escobedo-Morales, and Umapada Pal. "Thermolytic growth of ZnO nanocrystals: morphology control and optical properties." Crystal Growth and Design. 2008; 9(1):297-300.
19. Raja A, Ashokkumar S, Pavithra Marthandam R, Jayachandiran J, Chandra Prasad Khatiwada K, Kaviyarasu R, Ganapathi Raman, Swaminathan M. "Eco-friendly preparation of zinc oxide nanoparticles using Tabernaemontana divaricata and its photocatalytic and antimicrobial activity." *Journal of Photochemistry and Photobiology B: Biology*. 2018; 181:53-58.
20. Ramakanth K. Basics of diffraction and its application, I. K. International Publishing house PVT. LTD. New Dehli, 2007.
21. Sharma P, Sreenivas K, Rao KV. Analysis of ultraviolet photoconductivity in ZnO films prepared by unbalanced

magnetron sputtering. *Journal of Applied Physics*. 2003; 93(7):3963-3970.
22. Singh, Shubra, Ramachandra Rao MS. "Optical and electrical resistivity studies of isovalent and aliovalent 3 d transition metal ion doped ZnO." Physical Review B. 2009; 80(4):045210.
23. Sluiter, Marcel HF, Y. Kawazoe, Parmanand Sharma, A. Inoue, A. R. Raju, C. Rout, and U. V. Waghmare. "First principles based design and experimental evidence for a ZnO-based ferromagnet at room temperature." Physical review letters. 2005; 94(18):187204.
24. Sundaresan M, Yu ZX, Ferrans VJ, Irani K, Finkel T, Requirement for generation of H_2O_2 for platelet-derived growth factor signal transduction, Science, 1995, 270, 296-299.
25. Tam KH, A. B. Djurišić, C. M. N. Chan, Y. Y. Xi, C. W. Tse, Y. H. Leung, W. K. Chan, F. C. C. Leung, and D. W. T. Au. "Antibacterial activity of ZnO nanorods prepared by a hydrothermal method." Thin solid films. 2008; 516(18):6167-6174.
26. Tam, K. H., A. B. Djurišić, C. M. N. Chan, Y. Y. Xi, C. W. Tse, Y. H. Leung, W. K. Chan, F. C. C. Leung, and D. W. T. Au. "Antibacterial activity of ZnO nanorods prepared by a hydrothermal method." Thin solid films. 2008; 516(18):6167-6174.
27. Vijayaprasath G, Soundarrajan P, Ravi G. "The point defects induced ferromagnetism in ZnO semiconductor by terbium doping via co-precipitation method." *Journal of Materials Science: Materials in Electronics.* 2018; 2914):11892-11900.
28. Xiong, Gang U. Pal, J. G. Serrano, K. B. Ucer, and R. T. Williams. "Photoluminesence and FTIR study of ZnO nanoparticles: the impurity and defect perspective." physica status solidi c. 2006; 3(10): 3577-3581.
29. Yamamoto, Osamu. "Influence of particle size on the antibacterial activity of zinc oxide." *International Journal of Inorganic Materials*. 2001; 3(7):643-646.
30. Zandi S, Kameli P, Salamati H, Ahmadvand H, M. Hakimi. "Microstructure and optical properties of ZnO nanoparticles prepared by a simple method." Physica B: Condensed Matter. 2011; 406(17):3215-3218.
31. Zhou, Shengqiang, Kay Potzger, Helfried Reuther, Karsten Kuepper, Wolfgang Skorupa, Manfred Helm, and Juergen Fassbender. "Absence of ferromagnetism in V-implanted ZnO single crystals." *Journal of applied physics*. 2007; 101(9):09H109.